IEEE Access
Multidisciplinary ⋮ Rapid Review ⋮ Open Access Journal

Received March 5, 2022, accepted April 4, 2022, date of publication April 11, 2022, date of current version April 18, 2022.

Digital Object Identifier 10.1109/ACCESS.2022.3166629

Study on Calibration of 3-PR(4R)R Three-Degree-of-Freedom Parallel Mechanism

HAIBING FENG, JIAQING YAN, ZHENLIN JIN, AND ZIMING CHEN

Hebei Province Heavy Intelligent Manufacturing Equipment Technology Innovation Center, Yanshan University, Qinhuangdao, Hebei 066004, China
Heavy-Duty Intelligent Manufacturing Equipment Innovation Center of Hebei Province, Yanshan University, Qinhuangdao, Hebei 066004, China

Corresponding author: Zhenlin Jin (zljin@ysu.edu.cn)

This work was supported in part by the National Key Research and Development Program of China under Grant 2018YFB1308302, and in part by the National Natural Science Foundation of China under Grant 51775474.

ABSTRACT A kinematic calibration approach is proposed for a triple-planar 3-PR(4R)R parallel mechanism whose attitude error cannot be corrected by motion. First, the kinematic principle of the 3-PR(4R)R parallel mechanism is presented. Then, an error mapping function model is designed based on the mechanism's closed-loop vector equations. The model reveals the presence of coupling errors in the mechanism, i.e., the coupling of attitude and position errors, and is used to analyze error sensitivity as an indicator of component machining and assembly accuracy. A kinematic inverse solution is used to build a zero-point calibration and a full calibration method. Calibration is performed by a laser tracker-based calibration system, which generates much lower error values and delivers much improved accuracy. Experiments demonstrate that the proposed approach can potentially be used to calibrate parallel mechanisms with non-compensable error terms.

INDEX TERMS Parallel mechanism, error mapping, coupling error, calibration.

I. INTRODUCTION

Parallelmechanisms are often used for fine-tuning in practical engineering due to their high precision and high stability, and such fine-tuning mechanisms have been studied intensively by many researchers. Besides, six-degree-of-freedom (6-DOF) mechanisms are usually adopted for attitude adjustment due to their high stiffness, high precision, and high stability. An example is the automatic attitude adjustment system based on the Stewart 6-DOF robot and laser tracker coordinate measurement [1].

Parallel mechanisms are also a heated research topic in large attitude adjustment devices [2], such as the pointing platform of the James Webb telescope [3], the adjustment platform of the VLTI-ATS auxiliary telescope [4], and the secondary mirror adjustment platform of the VST telescope [5]. Many researchers have conducted theoretical studies on the parallel mechanisms for attitude adjustment. Tian L *et al.* [6] modeled and controlled the redundant parallel adjustment mechanism on deployable antenna panels. Ma, Z.-Q *et al.* [7] studied a 3-PPPS parallel mechanism for aircraft wing attitude adjustment to improve the efficiency of existing wing positioning systems in the acquisition of hinge points. Hsu, P. E. *et al.* [8] designed a seat adjustment mechanism based on the Stewart platform. Yao J [9] presented a Stewart platform-based mechanism to optimize and analyze the configuration of a parallel adjustment platform for satellite integrated assembly. To sum up, there has been an abundance of theoretical research on the use of the Stewart parallel mechanism with six degrees of freedom for attitude adjustment applications. Similarly, the 3-PR(4R)R three-degree-of-freedom (3-DOF) parallel mechanism in this paper can also be applied to fine tuning or attitude adjustment.

Many studies have been conducted on the calibration of parallel mechanisms. Using a 6-DOF parallel manipulator as the research structure model, Hu Y *et al.* [10] analyzed the geometric error sources that affected the reachable space of the mechanism and established a positional error mode to improve the motion accuracy of six-axis hybrid machine tools. Chu W *et al.* [11] proposed a calibration method for a redundant actuated parallel mechanism for attitude adjustment, and a calibration method based on force closed-loop feedback was used to calibrate each branch chain of the mechanism. Sun *et al.* [12] modeled the error of a 3-DOF parallel robot using the vector method. Frisoli *et al.* [13] modeled the error of a parallel robot in 3-URU space adopting

The associate editor coordinating the review of this manuscript and approving it for publication was Qingchun Chen.

spiral theory. In addition to the common methods mentioned above, G. Chen [14] also presented a parallel robot error modeling method based on the Product-of -Exponentials (POF) Formula.

In this paper, we explore a 3-PR(4R)R mechanism from the perspective of kinematic calibration. First, we develop a calibration algorithm based on the mechanism's characteristics and build a experimental calibration platform with a laser tracker. Next, we conduct theoretical and experimental analysis for zero-point calibration as well as full calibration. Finally, the accuracy of the fine-tuning mechanism is evaluated. Due to the error terms coupling of this mechanism and the characteristic that the attitude error is difficult to be compensated, the attitude error term is often ignored in the calibration process. The contributions of this paper : (1) error modeling for this mechanism, revealing the error term coupling; (2) a calibration model based on the kinematic inverse solution is established and calibration experiments are conducted for this mechanism to improve the motion accuracy of the mechanism.

II. KINEMATIC PRINCIPLE AND ERROR ANALYSIS

A. KINEMATIC PRINCIPLE

A sketch of the fine-tuning parallel mechanism is presented in Fig. 1. The mechanism is composed of two platforms and three branched chains with identical structures. The three branched chains containing closed-loop structures are evenly distributed between the fixed and moving platforms. Specifically, P denotes the moving sub and R denotes the rotating sub. The three branches of the moving sub $P_i(i = 1, 2, 3)$ are evenly distributed circumferentially on the fixed platform. The upper short side $A_{i1}A_{i2}$ of the parallelogram is connected to the moving sub slider by rotating sub R_{i1}, the lower short side $B_{i1}B_{i2}$ of the parallelogram is connected to the moving platform by rotating sub R_{i2}, and the four sides of the parallelogram $A_{i1}A_{i2}B_{i2}B_{i1}$ are connected by rotating sub R_{i3}, R_{i4}, R_{i5} and R_{i6}. The geometric relationships are $P_i \parallel R_{i1} \parallel R_{i2}$, $R_{i3} \parallel R_{i4} \parallel R_{i5} \parallel R_{i6}$, $R_{i1} \perp R_{i3}$.O is the point at which the three branches of R_{i1} meet, and O' is the point at which the three branches of R_{i2} meet.

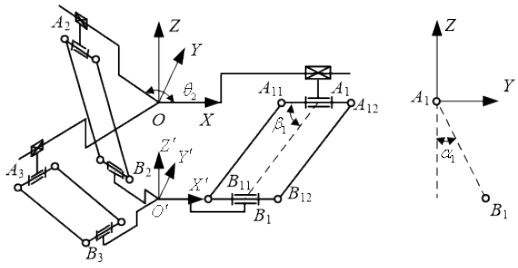

FIGURE 1. Simplified structure of 3-PR(4R)R mechanism.

The coordinate system of the mechanism is established, with point O taken as the origin of the fixed coordinate system, and the axis of R_{11} on the first branch chain as X-axis. The Z-axis is established perpendicularly to the fixed platform, being vertical upward, and Y-axis is determined by the right-hand rule. Point O' is set as the origin of the reference coordinate system of the moving platform and the axis of the rotating sub R_{12} on the first branch chain is taken as the X'-axis.The Z'-axis is established perpendicularly to the fixed platform, being vertical upward, and the Y' -axis is determined by the right-hand rule. A_1 is the midpoint of $A_{i1}A_{i2}$, and B_i is the midpoint of $B_{i1}B_{i2}$.

$l_i(i = 1, 2, 3)$ is defined as the length of OA_i, b as the length of $O'B_i$, h as the length of A_iB_i, and the angles θ_i between OAi and the positive direction of the X-axis of the fixed coordinate system $\{O\}$ as 0°, 120°, and 240°, respectively. The angle between the plane in which the parallelogram is located and the negative direction of the Z-axis is defined as $\alpha_i(i = 1, 2, 3)$, and the angle between A_iB_i and $A_{i1}A_{i2}$ is defined as $\beta_i(i = 1, 2, 3)$.

The coordinates of the output reference point O' of the mechanism in the fixed coordinate system $\{O\}$ are set as $\begin{bmatrix} x & y & z \end{bmatrix}^T$ and the vector closed-loop equation in the fixed coordinate system $\{O\}$ is established as:

$$\boldsymbol{r} = \boldsymbol{l}_i + \boldsymbol{h}_i - \boldsymbol{b}_i. \tag{1}$$

where $\boldsymbol{r} = OO', \boldsymbol{l}_i = OA_i, \boldsymbol{h}_i = A_iB_i, \boldsymbol{b}_i = O'B_i$.

Transformation of Equation (1) yields:

$$l_i = b + x\cos\theta_i + y\sin\theta_i \pm\sqrt{h^2 - z^2 - (x\sin\theta_i - y\cos\theta_i)^2} \tag{2}$$

The inverse solution of the position of the fine-tuning mecha- ism is obtained by rounding off the case where Equation (2) takes the minus sign:

$$l_i = b + x\cos\theta_i + y\sin\theta_i +\sqrt{h^2 - z^2 - (x\sin\theta_i - y\cos\theta_i)^2} \tag{3}$$

B. GEOMETRIC ERROR SOURCE ANALYSIS

Since the fine-tuning mechanism itself requires high accuracy, it is critical to establish an error model for the fine-tuning mechanism and conduct accuracy analysis to ensure the high accuracy of the system.

To establish a unified error model, the coordinate system of the mechanism is first defined as shown in Fig. 2.

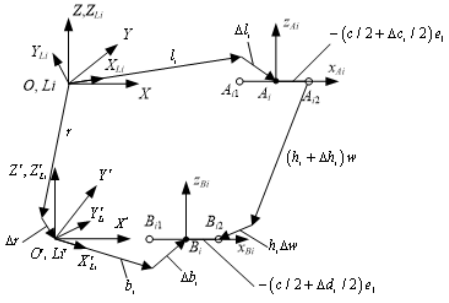

FIGURE 2. Error vector diagram of the fine-tuning mechanism.

The fixed coordinate system of the mechanism is defined as $O-XYZ$. The origin of the coordinate system O is located at the nominal intersection of the three branches $A_{11}A_{12}$,$A_{21}A_{22}$ and $A_{31}A_{32}$. The X-axis coincides with $A_{11}A_{12}$, and the Z-axis is perpendicular to the plane where $A_{11}A_{12}$, $A_{21}A_{22}$ and $A_{31}A_{32}$ are located. The Y-axis is determined according to the right-hand rule.

The conjoined coordinate system of the moving platform is defined as $O'-X'Y'Z'$. The origin of the coordinate system O' is located at the nominal intersection of the three branches of $B_{11}B_{12}$,$B_{21}B_{22}$ and $B_{31}B_{32}$. The X' axis coincides with $B_{11}B_{12}$, and the Z' axis is perpendicular to the plane where $B_{11}B_{12}$,$B_{21}B_{22}$ and $B_{31}B_{32}$ are located. The Y' axis is determined according to the right-hand rule.

The coordinate system of the driving branch is defined as $L_i-X_{Li}Y_{Li}Z_{Li}$, and the origin L_i of the driving branch's coordinate system coincides with the origin O of the fixed coordinate system.

The upper short side of the parallelogram near the conjoined coordinate system of the fixed platform $A_{i1}A_{i2}$ is defined as $A_i-x_{Ai}y_{Ai}z_{Ai}$. The origin of the coordinate system of the upper short side is point A_i. The x_{Ai} axis coincides with $A_{i1}A_{i2}$, and the y_{Ai} axis is parallel to the rotation sub-axis of this branch parallelogram. The z_{Ai} axis is determined according to the right-hand rule.

To describe the lower short side $B_{i1}B_{i2}$ of the parallelogram near the moving platform, the transition coordinate system $L_i'-X_{Li}'Y_{Li}'Z_{Li}'$ is established by means of rotating the conjoined coordinate system of the moving platform $O'-X'Y'Z'$ around the Z' axis by θ_i.

The lower short side of the parallelogram near the conjoined coordinate system of the moving platform $B_{i1}B_{i2}$ is defined as $B_i-x_{Bi}y_{Bi}z_{Bi}$. The origin of the lower short side coordinate system is the point B_i, and the x_{Bi} axis coincides with $B_{i1}B_{i2}$ the y_{Bi} axis is parallel to the rotation sub-axis of this branch parallelogram. The z_{Bi} axis is determined according to the right-hand rule.

The geometric error sources are defined as follows. The error of system $L_i-X_{Li}Y_{Li}Z_{Li}$ generated by the rotation of $O-XYZ$ around Z axis is defined as $\Delta\theta_{Ai}$; the error of the length of short side $A_{i1}A_{i2}$ is defined as Δc_i; the error in the driving branch for the rod length of the vector from point O_{Li} to point A_i is defined as $\Delta\boldsymbol{l}_i$; the attitude error of system $A_i-x_{Ai}y_{Ai}z_{Ai}$ generated by the rotation of the driving branch's coordinate system $L_i-X_{Li}Y_{Li}Z_{Li}$ around the X_{Li} axis is defined as $\Delta\boldsymbol{\alpha}_{Ai}$; the error of the length of the long side $A_{ij}B_{ij}$ is defined as Δh_{ij} ; the error of the unit direction vector of the long edge $A_{ij}B_{ij}$ is defined as $\Delta\boldsymbol{w_i}$; the error vector of the point O in system $O-XYZ$ is defined as $\Delta\boldsymbol{r}$; the attitude error vector of system $O'-X'Y'Z'$ with respect to the system $O-XYZ$ is defined as $\Delta\boldsymbol{\theta}$; the error of system $L_i'-X_{Li}'Y_{Li}'Z_{Li}'$ generated by the rotation of the dynamic system $O'-X'Y'Z'$ around the Z' axis is defined as $\Delta\theta_{Bi}$; length error of the lower short side $B_{i1}B_{i2}$ is defined as Δd_i; error vector from point L_i' to point B_i in system $L_i'-X_{Li}'Y_{Li}'Z_{Li}'$ is defined as $\Delta\boldsymbol{b_i}$; system $B_i-x_{Bi}y_{Bi}z_{Bi}$ is rotated by the transition coordinate system $L_i'-X_{Li}'Y_{Li}'Z_{Li}'$ around axis X_{Li}', and attitude state error is defined as $\Delta\boldsymbol{\alpha}_{Bi}$.

C. ESTABLISHMENT OF THE ERROR MAPPING FUNCTION

The vector equation of the branch closed-loop $O-L_i-A_i-A_{ij}-B_{ij}-B_i-L_i'-O'-O$ of the fine-tuning mechanism is:

$$\boldsymbol{r}={}^{O}_{Li}R\left(\boldsymbol{l}_i+\boldsymbol{c}_{ij}\right)+\boldsymbol{h}_{ij}-{}^{O}_{Li}R\left(\boldsymbol{b}_i+\boldsymbol{d}_{ij}\right) \tag{4}$$

where c_{ij} is the representation of the vector from point A_i to point A_{ij} in the coordinate system $L_i-X_{Li}Y_{Li}Z_{Li}$ of the driving branch,h_{ij} is the representation of the vector from point A_{ij} to point B_{ij} in the fixed coordinate system $O-XYZ$, and d_{ij} is the representation of the vector from point B_i to point B_{ij} in the transition coordinate system.

After the error is introduced, Equation (4) is subtracted under the small regression condition and the higher-order minimum is omitted, which yields:

$$\begin{aligned}\Delta\boldsymbol{r}=&{}^{O}_{Li}R\Delta\boldsymbol{e}_{1i}+sgn\,(j)\,{}^{O}_{Li}R\left({}^{Li}_{Ai}R\Delta e_{2i}/2\boldsymbol{e}_1+\Delta\boldsymbol{e}_{3i}{}^{Li}_{Ai}Rc/2\boldsymbol{e}_1\right)\\&+\Delta h_{ij}\boldsymbol{w}_i+h\Delta\boldsymbol{w}_i+\Delta\boldsymbol{\theta}_{Ai}{}^{O}_{Li}R\left[\boldsymbol{l}_i+sgn(j){}^{Li}_{Ai}Rc/2\boldsymbol{e}_1\right]\\&-\Delta\boldsymbol{\theta}_{Bi}{}^{O}_{Li}R\left[\boldsymbol{b}_i+sgn\,(j)\,{}^{Li}_{Ai}Rc/2\boldsymbol{e}_1\right]\\&-\Delta\boldsymbol{\theta}{}^{O}_{Li}R\left[\boldsymbol{b}_i+sgn\,(j)\,{}^{Li}_{Ai}Rc/2\boldsymbol{e}_1\right]\end{aligned} \tag{5}$$

where

$${}^{O}_{Li}R=\mathrm{Rot}\,(z,\theta_i)=\begin{bmatrix}\cos\theta_i & -\sin\theta_i & 0\\ \sin\theta_i & \cos\theta_i & 0\\ 0 & 0 & 1\end{bmatrix},$$

$${}^{Li}_{Ai}R=\mathrm{Rot}\,(x,\alpha_i)=\begin{bmatrix}1 & 0 & 0\\ 0 & \cos\alpha_i & -\sin\alpha_i\\ 0 & \sin\alpha_i & \cos\alpha_i\end{bmatrix},$$

$$sgn\,(j)=\begin{cases}-1 & j=1\\ 1 & j=2\end{cases},$$

$$\boldsymbol{e}_1=\begin{bmatrix}1&0&0\end{bmatrix}^T,$$

$$\Delta\boldsymbol{e}_{1i}=\Delta\boldsymbol{l}_i-\Delta\boldsymbol{b}_i,\ \Delta e_{2i}{=}\Delta c_i-\Delta d_i,\ \Delta\boldsymbol{e}_{3i}{=}\Delta\boldsymbol{\alpha}_{Ai}-\Delta\boldsymbol{\alpha}_{Bi}.$$

By multiplying both sides of the equal sign of Equation (5) by w_i and using the properties of the vector mixing product, we can get

$$\begin{aligned}\boldsymbol{w}_i^T\Delta\boldsymbol{r}=&\boldsymbol{w}_i^T{}^{O}_{Li}R\Delta\boldsymbol{e}_{1i}+sgn\,(j)\,\boldsymbol{w}_i^T{}^{O}_{Li}R{}^{Li}_{Ai}R\Delta e_{2i}/2\boldsymbol{e}_1\\&+sgn\,(j)\left({}^{Li}_{Ai}Rc/2\boldsymbol{e}_1\times\boldsymbol{w}_i\right)^T{}^{O}_{Li}R\Delta\boldsymbol{e}_{3i}+\Delta h_{ij}\\&+\left\{{}^{O}_{Li}R\left[\boldsymbol{l}_i+sgn\,(j)\,{}^{Li}_{Ai}Rc/2\boldsymbol{e}_1\right]\times\boldsymbol{w}_i\right\}^T\Delta\boldsymbol{\theta}_{Ai}\\&-\left\{{}^{O}_{Li}R\left[\boldsymbol{b}_i+sgn\,(j)\,{}^{Li}_{Ai}Rc/2\boldsymbol{e}_1\right]\times\boldsymbol{w}_i\right\}^T\Delta\boldsymbol{\theta}_{Bi}\\&-\left\{{}^{O}_{Li}R\left[\boldsymbol{b}_i+sgn\,(j)\,{}^{Li}_{Ai}Rc/2\boldsymbol{e}_1\right]\times\boldsymbol{w}_i\right\}^T\Delta\boldsymbol{\theta}\end{aligned} \tag{6}$$

As it can be seen from Equation(6), the position error and attitude error of the moving platform have a certain coupling relationship. With the fine-tuning mechanism only having three degrees of freedom for three-dimensional movement,

the resulting attitude error cannot be compensated by the motion.

By subtracting the closed-loop equations representing the error through different parallelogram long sides in the same branch, i.e., Equation (6) for $j = 2$ from Equation (6) for $j = 1$, and then making it ${}^{O}_{Li}R = \left[\, \boldsymbol{o}_{Li}\ \boldsymbol{n}_{Li}\ \boldsymbol{e}_3 \,\right]$ simplifies to:

$$\begin{aligned} c(\boldsymbol{o}_{Li} \times \boldsymbol{w}_i)^T \Delta\boldsymbol{\theta} = {} & \Delta e_{2i} \boldsymbol{w}_i^T \boldsymbol{o}_{Li} + c(\boldsymbol{e}_1 \times \boldsymbol{w}_i)^T {}^{O}_{Li}R \Delta\boldsymbol{e}_{3i} \\ & + \Delta h_{i2} - \Delta h_{i1} + c(\boldsymbol{o}_{Li} \times \boldsymbol{w}_i)^T \Delta\boldsymbol{\theta}_{Ai} \\ & - c(\boldsymbol{o}_{Li} \times \boldsymbol{w}_i)^T \Delta\boldsymbol{\theta}_{Bi} \end{aligned} \tag{7}$$

By writing Equation (7) in a matrix form, we can obtain the attitude error matrix function of the output of the dynamic platform of the fine-tuning mechanism:

$$\Delta\boldsymbol{\theta} = \boldsymbol{J}_{\theta\varepsilon} \Delta\boldsymbol{\varepsilon} \tag{8}$$

where

$$\begin{aligned} \boldsymbol{J}_{\theta\varepsilon} &= \boldsymbol{J}_{\theta A}^{-1} \boldsymbol{J}_{\theta B}, \boldsymbol{J}_{\theta A} = c\left[\boldsymbol{\rho}_{L1} \times \boldsymbol{w}\ \boldsymbol{\rho}_{L2} \times \boldsymbol{w}\ \boldsymbol{\rho}_{L3} \times \boldsymbol{w}_3 \,\right]^T, \\ \boldsymbol{J}_{\theta B} &= diag\left[\boldsymbol{J}_{\theta Bi}\right], \\ \boldsymbol{J}_{\theta Bi} &= \left[0_{1\times 3} \boldsymbol{w}_i^T \boldsymbol{o}_{Li} - 11 c(\boldsymbol{e}_1 \times \boldsymbol{w}_i)^T {}^{O}_{Li}R c(\boldsymbol{o}_{Li} \times \boldsymbol{w}_i)^T \right. \\ &\qquad \left. - c(\boldsymbol{o}_{Li} \times \boldsymbol{w}_i)^T \right], \\ \Delta\boldsymbol{\varepsilon} &= \left[\, \Delta\boldsymbol{\varepsilon}_1^T\ \Delta\boldsymbol{\varepsilon}_2^T\ \Delta\boldsymbol{\varepsilon}_3^T \,\right]^T, \\ \Delta\boldsymbol{\varepsilon}_i &= \left[\, \Delta\boldsymbol{\varepsilon}_{1i}^T\ \Delta e_{2i}\ \Delta h_{i1}\ \Delta h_{i2}\ \Delta\boldsymbol{e}_{3i}^T\ \Delta\boldsymbol{\theta}_{Ai}^T\ \Delta\boldsymbol{\theta}_{Bi}^T \,\right]^T. \end{aligned}$$

From Equation (8), 45 error sources can be observed, but not all of them have an effect on the attitude error in the output of the dynamic platform of the fine-tuning mechanism.

By adding the closed-loop equations representing the error through different parallelogram long sides in the same branch, i.e., Equation (6) for $j = 1$ and Equation (6) for $j = 2$, we can get:

$$\begin{aligned} \boldsymbol{w}_i^T \Delta\boldsymbol{r} = {} & \boldsymbol{w}_i^T {}^{O}_{Li}R \Delta\boldsymbol{e}_{1i} + \Delta h_{i1}/2 + \Delta h_{i2}/2 \\ & + \left({}^{O}_{Li}R\boldsymbol{l}_i \times \boldsymbol{w}_i\right)^T \Delta\boldsymbol{\theta}_{Ai} - \left({}^{O}_{Li}R\boldsymbol{b}_i \times \boldsymbol{w}_i\right)^T \Delta\boldsymbol{\theta}_{Bi} \\ & - c(\boldsymbol{o}_{Li} \times \boldsymbol{w}_i)^T \Delta\boldsymbol{\theta}_{Bi} \end{aligned} \tag{9}$$

Equation (9) is written in a matrix form to obtain the attitude error matrix function of the output of the dynamic platform of the fine-tuning mechanism:

$$\Delta\boldsymbol{r} = \boldsymbol{J}_{rC}^{-1} \boldsymbol{J}_{rD} \Delta\boldsymbol{\varepsilon} + \boldsymbol{J}_{rC}^{-1} \boldsymbol{J}_{r\theta} \boldsymbol{J}_{\theta\varepsilon} \Delta\boldsymbol{\varepsilon} = \boldsymbol{J}_{r\varepsilon} \Delta\boldsymbol{\varepsilon} \tag{10}$$

where

$$\begin{aligned} \boldsymbol{J}_{r\varepsilon} &= \boldsymbol{J}_{rC}^{-1} \boldsymbol{J}_{rD} + \boldsymbol{J}_{rC}^{-1} \boldsymbol{J}_{r\theta} \boldsymbol{J}_{\theta\varepsilon}, \boldsymbol{J}_{rC} = \left[\, \boldsymbol{w}_1\ \boldsymbol{w}_2\ \boldsymbol{w}_3 \,\right]^T, \\ \boldsymbol{J}_{rDi} &= \left[\boldsymbol{w}_i^T {}^{O}_{Li}R 0\ 1/2 1/2 0_{1\times 3}\ \left({}^{O}_{Li}R\boldsymbol{l}_i \times \boldsymbol{w}_i\right)^T - \left({}^{O}_{Li}R\boldsymbol{b}_i \times \boldsymbol{w}_i\right)^T\right], \\ \boldsymbol{J}_{r\theta} &= -\left[\, {}^{O}_{L1}R\boldsymbol{b}_1 \times \boldsymbol{w}_1\ {}^{O}_{L2}R\boldsymbol{b}_2 \times \boldsymbol{w}_2\ {}^{O}_{L3}R\boldsymbol{b}_3 \times \boldsymbol{w}_3 \,\right]^T. \end{aligned}$$

From Equation (10), it can be observed that not all the mechanism errors have a direct effect on the position error of the moving platform in the fine-tuning mechanism, except for the attitude error $\Delta\boldsymbol{\theta}$ of the moving platform. $\boldsymbol{J}_{rDi}$ in the columns corresponding to error sum Δe_{2i} and $\Delta\boldsymbol{e}_{3i}$ is 0, which means that there is no direct effect on the position error. However, from Equation (8), it can be observed that the errors Δe_{2i} and $\Delta\boldsymbol{e}_{3i}$ have an effect on the attitude error $\Delta\boldsymbol{\theta}$ of the moving platform, which indirectly affects the position error of the moving platform. This indicates that the coupling of attitude error and position error of the moving platform causes all error sources to have an effect on the position error of the moving platform.

D. ERROR SENSITIVITY ANALYSIS

The mean and standard deviation of the sensitivity of the attitude error source over the entire operating space are used as a comprehensive criterion for evaluating error sensitivity:

$$\begin{cases} \mu_{\lambda\theta i} = \dfrac{\int_{V_t} \lambda_{\theta i} dV_t}{V_t} \\ \sigma_{\lambda\theta i} = \sqrt{\dfrac{\int_{V_t} (\sigma_{\lambda\theta i} - \mu_{\lambda\theta i})^2 dV_t}{V_t}} \end{cases} \tag{11}$$

where $\mu_{\lambda\theta i}$ is the mean value of the local sensitivity λ_{ri} of the position error over the entire operating space, and $\sigma_{\lambda ri}$ is the standard deviation of the local sensitivity λ_{ri} of the position error over the entire operating space.

We use the mean and standard deviation of local sensitivity over the entire operating space as a comprehensive criterion for evaluating error sensitivity:

$$\begin{cases} \mu_{\lambda ri} = \dfrac{\int_{V_t} \lambda_{ri} dV_t}{V_t} \\ \sigma_{\lambda ri} = \sqrt{\dfrac{\int_{V_t} (\sigma_{\lambda ri} - \mu_{\lambda ri})^2 dV_t}{V_t}} \end{cases} \tag{12}$$

where is $\mu_{\lambda ri}$ the mean value of the local sensitivity λ_{ri} of the position error over the entire operating space, and $\sigma_{\lambda ri}$ is the standard deviation of the local sensitivity λ_{ri} of the position error over the entire operating space.

First, by traversing all positions in this operating space, local sensitivities $\lambda_{\theta i}$ and λ_{ri} are calculated. Then, using Equations (11) and (12), global error sensitivity analysis is performed on each error source of the fine-tuning mechanism. Finally, the nominal values of each mechanism parameter are calculated based on the values given in Table 1. The results are represented by the error bar graph shown in Fig. 3.

TABLE 1. Initial values temporarily given for each parameter of the fine-tuning mechanism.

Mechanism parameters	Parameter value
b / mm	180
h / mm	260
l_i / mm	[280, 430]

As analyzed with Fig. 3, it can be known that the sensitivities of the attitude error and position error at the end of the fine-tuning mechanism about the distance error source in $\Delta\boldsymbol{e}_1$ are relatively small, and the sensitivities of both Δh_1 and Δh_2 are relatively large. The position error about the angle error source of the fine-tuning mechanism is more sensitive to $\Delta\boldsymbol{\theta}_A$

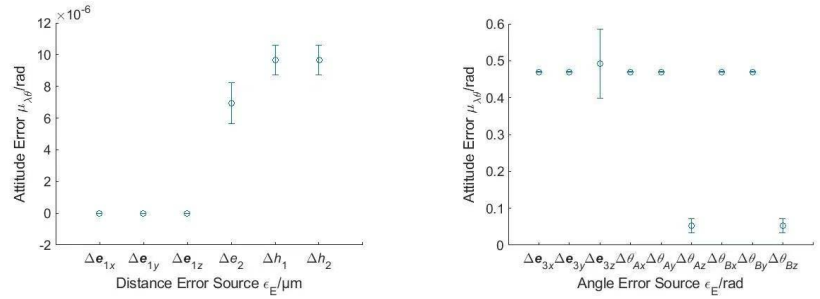

(a) Sensitivity of attitude error to distance error sources (b) Sensitivity of attitude error to angular error sources

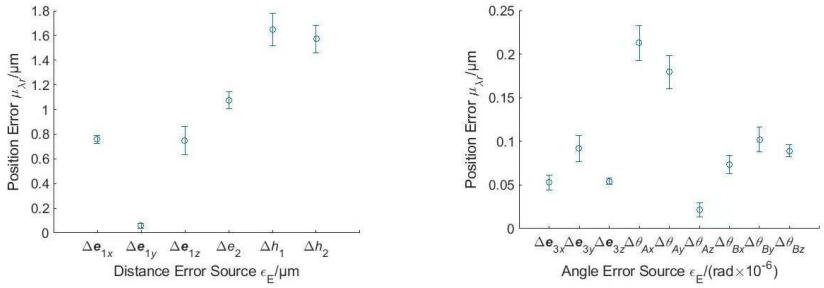

(c) Sensitivity of position error to distance error sources (d) Sensitivity of position error to angular error sources

FIGURE 3. Sensitivity of each error of the fine-tuning mechanism.

than it is to $\Delta\boldsymbol{\theta}_B$. If the standard deviation of the attitude error $\Delta\theta$ caused by the error source Δh_1 is expected to be kept no greater than 20 μm/m, the tolerance of h_1 must be better than $T(h_1) = \pm 3 \times 20/9.66 = \pm 6.21$ μm; if the standard deviation of the position error Δr caused by the error source Δh_1 is expected to be kept no greater than 20μm, the tolerance of parameter h_1 must reach $T(h_1) = \pm 3 \times 20/1.65 = \pm 36$ μm; if the standard deviation of the position error Δr caused by the desired error source $\Delta\theta_{Ax}$ is expected to be kept no greater than 20μm, the tolerance of this parameter can be relaxed to $T(h_1) = \pm 3 \times 20/0.2128 = \pm 282$ μm/m.

III. CALIBRATION PRINCIPLES AND EXPERIMENTAL STUDIES

A. ANALYSIS OF CALIBRATION PRINCIPLE

The principle of kinematic calibration is to identify the error between the theoretical value of each parameter in the kinematic model and the actual value of each parameter in the real mechanism, and then compensate the error to the control system, so as to improve the motion accuracy of the mechanism. Generally, the kinematic calibration process involves these steps: establishing an error model, collecting experimental data, identifying the mechanism parameters, compensating the control parameters, and verifying the identification performance. In this part of the study, the error model is established based on the kinematic inverse solution.

B. ZERO CALIBRATION PRINCIPLE AND ALGORITHM

The derived inverse solution of Equation (3) in a general form as:

$$\boldsymbol{l} = f\left(\boldsymbol{O'},\ \boldsymbol{\psi}\right) \tag{13}$$

where $\boldsymbol{l}$ is the input parameter, $\boldsymbol{O'}$ is the end output positional data, $\boldsymbol{\psi}$ is the mechanism parameters included in the inverse solution, and $f\left(\boldsymbol{O'},\ \boldsymbol{\psi}\right)$ is the kinematic inverse solution.

Using the inverse solution of Equation (8), the error between the theoretical value and the true value for the jth position data can be obtained as:

$$\Delta\boldsymbol{l}_j = \boldsymbol{l}_j - f\left(\boldsymbol{O'}_{mj},\ \boldsymbol{\psi}_r\right) \tag{14}$$

where $\Delta\boldsymbol{l}_j$ is the error between the theoretical value and the true value of the jth position, $\boldsymbol{O'}_{mj}$ is the measured position data at the jth position, $\boldsymbol{\psi}_r$ is the true value of the mechanism parameters included in the inverse solution, and $\boldsymbol{l}_j$ is the actual input parameters at the jth position.

The following formula is used to calculate the actual input parameter $\boldsymbol{l}_j$ of the fine-tuning mechanism at the jth position:

$$\boldsymbol{l}_j = f\left(\boldsymbol{O'}_{tj},\ \boldsymbol{\psi}_t\right) \tag{15}$$

where $\boldsymbol{O'}_{tj}$ is the theoretical positional data output from the end of the mechanism at the jth position, and $\boldsymbol{\psi}_t$ is the theoretical value of the mechanism parameters included in the kinematic inverse solution of the fine-tuning mechanism.

The kinematic calibration process of the fine-tuning mechanism is to make the error infinitely close to zero based on the following branch construction equation:

$$\Delta l_{ij} = L_{ij}\left(l_{i0},\ \boldsymbol{\psi}_r\right) = l_{i0} + l_{ij} - f\left(\boldsymbol{O'}_{mj},\ \boldsymbol{\psi}_r\right) = 0 \tag{16}$$

where Δl_{ij} is the error of the moving sub position of the ith branch chain at the jth position, L_{ij} is the error function of the ith branch chain at the jth position, l_{i0} is the initial value of the moving sub position of the ith branch chain, and l_{ij} is the changed value of the moving sub position of the ith branch chain at the jth position.

From Equation (16), it can be seen that the independent variables of the error function include two parts: the initial value of the position of the moving sub of the fine-tuning mechanism l_{i0}, and the mechanism parameters of the fine-tuning mechanism $\boldsymbol{\psi}_r$.

If only zero calibration is performed on the mechanism, it can be seen from Equation (16) that the independent variables of the three error functions l_{ij} $(i = 1, 2, 3)$ corresponding to the jth position include three unknowns l_{i0} $(i = 1, 2, 3)$, and theoretically, only one change is needed to fine-tune the position of the mechanism. To ensure the error of the actual measurement data does not influence the zero calibration process, it is necessary to increase the number of measurements. The zero calibration process after multiple measurements are considered will make the initial value of the mechanism input closer to the true value, thus improving the motion accuracy of the mechanism.

Assuming that the positional data of n fine-tuning mechanisms are measured, $3n$ independent equations can be obtained as:

$$\begin{cases} L_{11}(l_{10}) = 0; & L_{21}(l_{20}) = 0; & L_{31}(l_{30}) = 0 \\ L_{12}(l_{10}) = 0; & L_{22}(l_{20}) = 0; & L_{32}(l_{30}) = 0 \\ \cdots & \cdots & \cdots \\ L_{1n}(l_{10}) = 0; & L_{2n}(l_{20}) = 0; & L_{3n}(l_{30}) = 0 \end{cases} \tag{17}$$

Therefore, the zero calibration problem of the fine-tuning mechanism is transformed into the problem of solving the optimal solution of a nonlinear system of equations including Equation (17). Specifically, the number of equations is much greater than the number of unknowns, and the nonlinear least-squares method is usually used to find the optimal solution of the system of equations.

C. FULL CALIBRATION PRINCIPLE AND ALGORITHM

If the mechanism is to be fully calibrated, it is known from Equation (16) that the three error functions $l_{ij}(i = 1, 2, 3)$ corresponding to the jth position contain nine independent variables. Therefore, theoretically only three changes are needed to fine-tune the mechanism's position. To ensure the error of the actual measurement data does not influence the full calibration process, it is necessary to increase the number of measurements. The full calibration process after multiple measurements are considered will make the initial value of the mechanism input closer to the true value, thus improving the motion accuracy of the mechanism.

Assuming that the positional data of n fine-tuning mechanisms are measured, $3n$ independent equations can be obtained as (18), shown at the bottom of the page.

Similarly, the full calibration problem of the fine-tuning mechanism is transformed into the problem of solving the optimal solution of a nonlinear system of equations including Equation (18). Specifically, the number of equations is much greater than the number of unknowns, and the nonlinear least-squares method is usually used to find the optimal solution of the system of equations.

D. CALIBRATION SYSTEM CONSTRUCTION AND CALIBRATION EXPERIMENTS

The built calibration experiment system is shown in Figure 4.

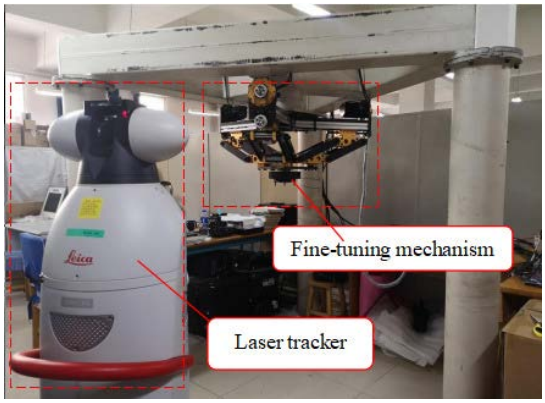

FIGURE 4. Calibration experimental system.

In the experimental calibration system, the coordinate system of the laser tracker is set as the measurement coordinate system $\{M\}$, with the fixed coordinate system $\{O\}$ of the fine-tuning mechanism fixed to the fixed platform and the motion coordinate system $\{O'\}$ fixed to the moving platform. In the measurement process, it is difficult to measure the kinematic system of the fine-tuning mechanism directly. Therefore, a fixed point P is introduced on the moving platform as an auxiliary measurement point, through which the position of the kinematic system is measured. The position relationship between the three coordinate systems is shown in Fig. 5. Through calibration experiments, the position of the origin of the moving platform in the fixed system $\{O\}$ is calculated, and according to the position relationship shown

$$\begin{cases} L_{11}\left(l_{10}\ h_1\ \theta_1\right) = 0; & L_{21}\left(l_{20}\ h_2\ \theta_2\right) = 0; & L_{31}\left(l_{30}\ h_3\ \theta_3\right) = 0 \\ L_{12}\left(l_{10}\ h_1\ \theta_1\right) = 0; & L_{22}\left(l_{20}\ h_2\ \theta_2\right) = 0; & L_{32}\left(l_{30}\ h_3\ \theta_3\right) = 0 \\ \cdots & \cdots & \cdots \\ L_{1n}\left(l_{10}\ h_1\ \theta_1\right) = 0; & L_{2n}\left(l_{20}\ h_2\ \theta_2\right) = 0; & L_{3n}\left(l_{30}\ h_3\ \theta_3\right) = 0 \end{cases} \tag{18}$$

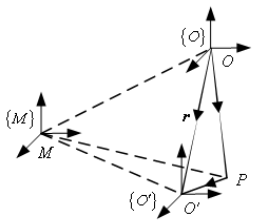

FIGURE 5. Measuring coordinate system.

in Fig. 5, we can get:

$$\boldsymbol{r} = \boldsymbol{OP} + \boldsymbol{PO'} \tag{19}$$

where $\boldsymbol{r}$ is the representation of vector $\boldsymbol{OO'}$ in system $\{O\}$, $\boldsymbol{OP}$ is the representation of the vector of point P in the system $\{O\}$, and $\boldsymbol{PO'}$ is the representation of the vector of point P to the origin $\{O'\}$ of the dynamic system of the fine-tuning mechanism in system $\{O\}$.

Since the data measured in the measurement system are represented in the laser tracker's coordinate system $\{M\}$, the data in Equation (19) are transformed into the laser tracker's coordinate system $\{M\}$, which is obtained from the coordinate transformation formula:

$$\boldsymbol{OP} = {}^{O}_{M}\boldsymbol{R}\left({}^{M}\boldsymbol{P} - {}^{M}\boldsymbol{O}\right), \boldsymbol{PO'} = {}^{O}_{M}\boldsymbol{R}{}^{M}\boldsymbol{PO'} \tag{20}$$

where ${}^{O}_{M}\boldsymbol{R}$ is the rotation matrix from system $\{M\}$ to system $\{O\}$, ${}^{M}P$ is the vector representation of point P in system $\{M\}$, ${}^{M}\boldsymbol{O}$ is the vector representation of the fixed system's origin O in system $\{M\}$, and ${}^{M}\boldsymbol{PO'}$ is the representation of the vector $\boldsymbol{PO'}$ in system $\{M\}$.

Substituting Equation (20) into Equation (19) yields:

$$\boldsymbol{r} = {}^{O}_{M}\boldsymbol{R}\left({}^{M}\boldsymbol{P} - {}^{M}\boldsymbol{O}\right) + {}^{O}_{M}\boldsymbol{R}{}^{M}PO' \tag{21}$$

As analyzed above, it is necessary to measure the fixed coordinate system $\{O\}$, including the position of its origin O in system $\{M\}$, the position of point P in system $\{M\}$, and the position of the origin O' of the fine-tuning mechanism's motion coordinate system in system $\{M\}$. The position of each of the measurement points is shown in Fig. 6.

Table 2 shows the three sets of data for the auxiliary measurement point P.

The coordinate system data of the fixed platform of the fine-tuning mechanism and the value of vector ${}^{M}\boldsymbol{PO'}$ can be obtained as follows by fitting the calculation:

$${}^{M}_{O}R = \begin{bmatrix} 0.530648 & -0.847574 & -0.005559 \\ 0.847556 & 0.530674 & -0.005868 \\ 0.007923 & -0.001598 & 0.999967 \end{bmatrix}, \tag{22}$$

$${}^{M}O = \begin{bmatrix} 1884.021187 \\ 30.760965 \\ 115.522375 \end{bmatrix}.$$

TABLE 2. Data of auxiliary measuring point P.

Group		x	y	z
Group 1	1	1838.081154	-136.146847	-21.375013
	2	1836.348089	-138.945944	-24.888753
	...	...	...	...
	15	1812.366651	-177.906482	-57.930659
Group 2	1	1838.082599	-136.145954	-21.377125
	2	1841.444856	-136.206068	-24.859075
	...	...	...	...
	15	1887.829282	-137.133139	-57.399779
Group 3	1	1838.080897	-136.148985	-21.372618
	2	1836.503684	-133.184228	-24.846956
	...	...	...	...
	15	1814.690363	-92.539718	-57.346104

TABLE 3. Zero calibration result.

Parameters	Theoretical values	Calibrated value
l_{10}/mm	410	410.004 05
l_{20}/mm	410	408.679 26
l_{30}/mm	410	410.469 35

$${}^{M}\boldsymbol{PO'} = \begin{bmatrix} 47.583753 \\ 167.196757 \\ 27.233236 \end{bmatrix} \tag{23}$$

E. ZERO CALIBRATION RESULTS

With the data for auxiliary measurement point P in Table 2, Equation (22) and Equation (23) are substituted into Equation (21) to obtain the actual value r output from the fine-tuning mechanism. Then, the actual value obtained from this measurement and the corresponding command input value of the mechanism are substituted into Equation (17) to obtain the zero calibration results of the fine-tuning mechanism, as shown in Table 3.

F. FULL CALIBRATION RESULTS

The actual value r obtained from the measurement and the corresponding command input value of the mechanism are substituted into Equation (18) to obtain the full calibration results of the fine-tuning mechanism, as shown in Table 4.

TABLE 4. Full calibration result.

Parameters	Theoretical values	Calibrated value
l_{10}/mm	410	410.004 05
l_{20}/mm	410	408.679 26
l_{30}/mm	410	410.469 35
h_1/mm	260	260.006 487
h_2/mm	260	260.139 361
h_2/mm	260	261.235 727
θ_1/°	0	0.312 582
θ_2/°	120	120.594 854
θ_3/°	240	240.698 283

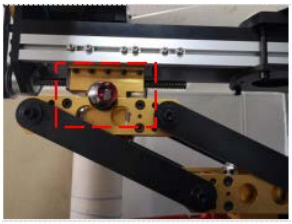

(a) The 1st axis of the fixed platform

(b) Outside of 1st axis of the moving platform

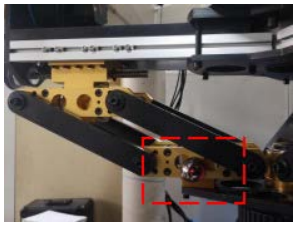

(c) Inside of the 1st axis of the moving platform

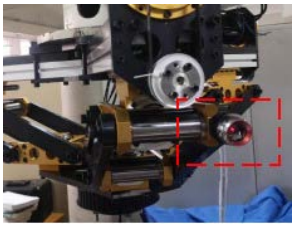

(d) The 2nd axis of the fixed platform

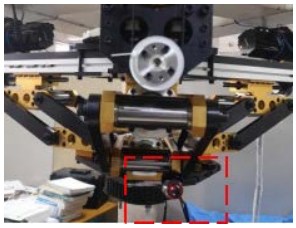

(e) Outside of the 2nd axis of the moving platform

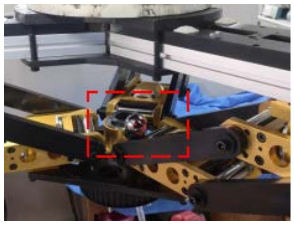

(f) Inside of the 2nd axis of the moving platform

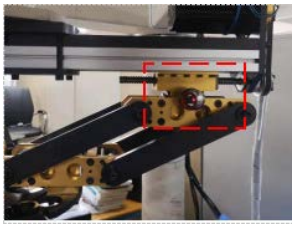

(g) The 3rd axis of the fixed platform

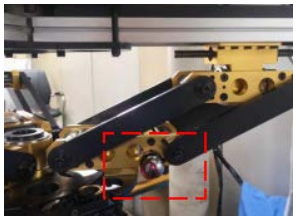

(h) Outside of the 3rd axis of the moving platform

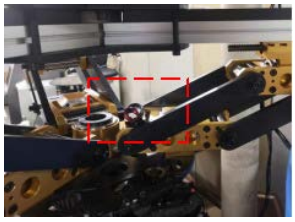

(i) Inside of the 3rd axis of the moving platform

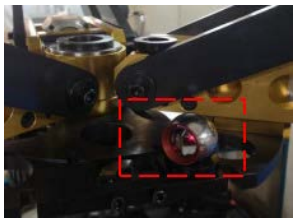

(j) Position of point P on the moving platform

FIGURE 6. Location of each measuring point.

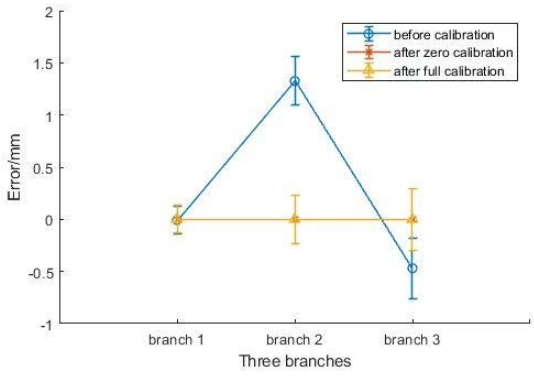

FIGURE 7. Comparison of errors before and after calibration.

Fig. 7 compares the errors of the moving sub positions before and after calibration in an error bar graph. Specifically, the marked points represent the mean error values and the ranges the standard deviations of the errors. From Fig. 7, it can be seen that the errors of the three branches become closer to the mean error value of 0 after zero calibration or full calibration. Branch 2 exhibits the most obvious change in the mean error value, dropping from 1.320 740 mm before calibration to $1.263\ 188 \times 10^{-14}$ mm after zero calibration, and to $1.263\ 187 \times 10^{-14}$ mm after full calibration. Branch 1 exhibits a very small data variation, which indicates that the initial value of Branch 1 is closer to the real value.

IV. ACCURACY EVALUATION

A. POSITION ACCURACY AND POSITION REPEATABILITY EVALUATION

The position accuracy and position repeatability of the fine-tuning mechanism before and after calibration are shown in Table 5 and Table 6. In this paper, the largest position accuracy and position repeatability values obtained after

TABLE 5. Position accuracy before and after calibration.

Measurement point	Before calibration				After calibration			
	AP_P	AP_x	AP_y	AP_z	AP_P	AP_x	AP_y	AP_z
P_1	1.1154	0.35693	-0.98904	-0.3722	0.41367	-0.06441	0.40707	-0.03572
P_2	1.3581	0.61745	-1.1092	-0.4827	0.40186	-0.01468	0.38916	-0.09915
P_3	1.2327	0.14127	-1.1749	-0.3452	0.31053	-0.05834	0.28625	0.10529
P_4	0.96163	0.08705	-0.91365	-0.28707	0.42391	-0.11974	0.40626	0.01779
P_5	1.0498	0.57453	-0.79873	-0.3662	0.59132	-0.08824	0.5634	-0.15638

TABLE 6. Position repeatability before and after calibration.

Measurement point	P_1	P_2	P_3	P_4	P_5
Before calibration	0.00969	0.010445	0.008529	0.008663	0.008364
After calibration	0.005516	0.007261	0.005415	0.006182	0.008164

TABLE 7. Position distance accuracy before and after calibration.

Item	AD_P	AD_x	AD_y	AD_z
Before calibration	-0.30457	-0.17351	-0.17485	-0.17917
After calibration	-0.11983	-0.066524	-0.068883	-0.072139

TABLE 8. Position distance repeatability before and after calibration.

Item	RD	RD_x	RD_y	RD_z
Before calibration	±0.49544	±0.286	±0.28638	±0.28575
After calibration	±0.14463	±0.083573	±0.083859	±0.083122

calibration are taken as the final position accuracy and position repeatability of the fine-tuning mechanism, i.e., 0.59132 mm for position accuracy and 0.008164 mm for position repeatability.

B. POSITION DISTANCE ACCURACY EVALUATION AND POSITION DISTANCE REPEATABILITY EVALUATION

The position distance accuracy and position distance repeatability results of the fine-tuning mechanism before and after calibration are shown in Table 7 and Table 8. In this paper, the largest position distance accuracy and position distance repeatability values obtained after calibration are taken as the final position distance accuracy and position distance repeatability of the fine-tuning mechanism, i.e., -0.11983 mm for position distance accuracy and ± 0.14463 mm for position distance repeatability.

V. DISCUSSION OF THE RESULTS

As revealed by the comparative data in Table 5, Table 6, Table 7, and Table 8, the position accuracy, position repeatability, position distance accuracy, and position distance repeatability of the fine-tuning mechanism are improved significantly after calibration. This means that the calibration performance is remarkable and the fine-tuning mechanism meets the requirements for use in terms of each indicator.

VI. CONCLUSION

In this paper, we analyze the kinematic principle of a 3-PR(4R)R 3-DOF fine-tuning mechanism by the position inverse solution of the mechanism, analyze the error sources, establish an error mapping function, and then analyze the sensitivities of the error sources. The kinematic calibration principle is applied to establish a zero calibration model and a full calibration model. The measurement principle of the laser tracker is proposed to build an experimental calibration platform, and the error value is reduced significantly. After calibration, the position accuracy, position repeatability, position distance accuracy, and position distance repeatability of the fine-tuning mechanism are 0.59132 mm, 0.008164 mm, -0.11983 mm, and ± 0.14463 mm. These results suggest that the proposed approach delivers remarkable calibration performance and significantly improved accuracy. The proposed approach offers an inspiring means of calibrating parallel mechanisms with non-compensable error items.

REFERENCES

[1] W. Wei, J. Li, and S. Ma, "Automatic adjustment system for space position and attitude of complex structural parts," in *Proc. IEEE Int. Conf. Inf. Technol., Big Data Artif. Intell. (ICIBA)*, Chongqing, China, Nov. 2020, pp. 1100–1104.

[2] J. Yao, B. Han, Y. Dou, Y. Xu, and Y. Zhao, "Fault-tolerant strategy and workspace of the subreflector parallel adjusting mechanism," *Proc. Inst. Mech. Eng. C, J. Mech. Eng. Sci.*, vol. 233, no. 18, pp. 6656–6667, Jul. 2019.

[3] J. Nella *et al.*, "James Webb space telescope (JWST) observatory architecture and performance," *Proc. SPIE*, vol. 5487, pp. 576–587, Oct. 2004.
[4] L. Zago and S. Droz, "Small parallel manipulator for the active alignment and focusing of the secondary mirror of the VLTI ATS," *Proc. SPIE*, vol. 4003, no. 4, pp. 450–455, 2000.
[5] P. Schipani, S. D'Orsi, D. Fierro, L. Marty, F. Perrotta, and C. Arcidiacono, "Performance of the VST secondary mirror support system," *Proc. SPIE*, vol. 7739, Jul. 2010, Art. no. 773932.
[6] L. Tian, H. Bao, M. Wang, and X. Duan, "Modeling and control of the redundant parallel adjustment mechanism on a deployable antenna panel," *Sensors*, vol. 16, no. 10, p. 1632, Oct. 2016.
[7] Z. Ma, S. G. Li, H. Xing, and H. Xiang, "Analytic forward solution for 3-PPPS parallel wing posture adjustment mechanism," *Comput. Integr. Manuf. Syst.*, vol. 21, no. 2, pp. 449–454, 2015.
[8] P. E. Hsu, Y. L. Hsu, J. M. Lu, and C.-H. Chang, "Seat adjustment design of an intelligent robotic wheelchair based on the Stewart platform," *Int. J. Adv. Robot. Syst.*, vol. 10, no. 3, p. 168, Jan. 2013.
[9] J. Yao, G. Wu, and Y. Zhao, "Configuration optimization and analysis of the parallel adjustment platform for satellite integrated assembly," in *Proc. 11th IEEE Int. Conf. Ind. Informat. (INDIN)*, Bochum, Germany, Jul. 2013, pp. 317–320.
[10] Y. Hu, F. Gao, X. Zhao, B. Wei, D. Zhao, and Y. Zhao, "Kinematic calibration of a 6-DOF parallel manipulator based on identifiable parameters separation (IPS)," *Mech. Mach. Theory*, vol. 126, pp. 61–78, Aug. 2018.
[11] W. Chu, X. Huang, and S. Li, "A calibration method of redundant actuated parallel mechanism for posture adjustment," *Ind. Robot, Int. J. Robot. Res. Appl.*, vol. 48, no. 4, pp. 494–509, Apr. 2021.
[12] T. Sun, Y. Song, Y. Li, and L. Xu, "Separation of comprehensive geometrical errors of a 3-DOF parallel manipulator based on Jacobian matrix and its sensitivity analysis with Monte–Carlo method," *Chin. J. Mech. Eng.* vol. 24, no. 3, p. 406, Mar. 2011.
[13] A. Frisoli, M. Solazzi, D. Pellegrinetti, and M. Bergamasco, "A new screw theory method for the estimation of position accuracy in spatial parallel manipulators with revolute joint clearances," *Mech. Mach. Theory*, vol. 46, no. 12, pp. 1929–1949, Dec. 2011.
[14] G. Chen, L. Kong, Q. Li, H. Wang, and Z. Lin, "Complete, minimal and continuous error models for the kinematic calibration of parallel manipulators based on POE formula," *Mech. Mach. Theory*, vol. 121, pp. 844–856, Mar. 2018.
[15] T. Huang, D. G. Chetwynd, D. J. Whitehouse, and J. Wang, "A general and novel approach for parameter identification of 6-DOF parallel kinematic machines," *Mech. Mach. Theory*, vol. 40, no. 2, pp. 219–239, Feb. 2005.
[16] L. Yang, X. Tian, Z. Li, F. Chai, and D. Dong, "Numerical simulation of calibration algorithm based on inverse kinematics of the parallel mechanism," *Optik*, vol. 182, pp. 555–564, Apr. 2019.
[17] T. Li, F. Li, Y. Jiang, J. Zhang, and H. Wang, "Kinematic calibration of a 3-P(Pa)S parallel-type spindle head considering the thermal error," *Mechatronics*, vol. 43, pp. 86–98, May 2017.
[18] J.-F. Wu, R. Zhang, R.-H. Wang, and Y.-X. Yao, "A systematic optimization approach for the calibration of parallel kinematics machine tools by a laser tracker," *Int. J. Mach. Tools Manuf.*, vol. 86, pp. 1–11, Nov. 2014.
[19] C. Fan, G. Zhao, J. Zhao, L. Zhang, and L. Sun, "Calibration of a parallel mechanism in a serial-parallel polishing machine tool based on genetic algorithm," *Int. J. Adv. Manuf. Technol.*, vol. 81, nos. 1–4, pp. 27–37, May 2015.
[20] A. Klimchik, A. Pashkevich, D. Chablat, and G. Hovland, "Compliance error compensation technique for parallel robots composed of non-perfect serial chains," *Robot. Comput.-Integr. Manuf.*, vol. 29, no. 2, pp. 385–393, Apr. 2013.
[21] K. Balaji and H. K. B. Shaul, "Kinematic analysis of novel 3RRS parallel mechanism," *Int. J. Sci. Res.*, vol. 7, no. 1, pp. 111–114, 2018.
[22] T. A. Hess-Coelho, G. E. E. Gojtan, and G. P. Furtado, "Kinematic analysis of a 3-DOF parallel mechanism for milling applications," *Open Mech. Eng. J.*, vol. 4, no. 1, pp. 69–76, Feb. 2010.
[23] A. A. Selvakumar and M. A. Kumar, "Experimental investigation on position analysis of 3–DOF parallel manipulators," *Proc. Eng.*, vol. 97, pp. 1126–1134, Jan. 2014.
[24] A. Joubair, L. F. Zhao, P. Bigras, and I. Bonev, "Absolute accuracy analysis and improvement of a hybrid 6-DOF medical robot," *Ind. Robot, Int. J.*, vol. 42, no. 1, pp. 44–53, Jan. 2015.
[25] Y. C. Yuan and Y. Zhang, "Building of fine-tuning mechanism posture and kinematics model for shield segment erector," in *Advanced Materials Research*, vol. 634. Düsseldorf, Germany: Trans Tech Publications, 2013, pp. 3737–3740.

HAIBING FENG received the B.S. and M.S. degrees in mechanical engineering from Yanshan University, Qinhuangdao, China, in 2004 and 2009, respectively, where he is currently pursuing the Ph.D. degree in mechanical engineering. He is also engaged in research and development on parallel manipulator, parallel kinematic machine, and their applications.

JIAQING YAN was born in Nantong, Jiangsu, China, in 1998. He received the B.S. degree in mechanical engineering from Yanshan University, in 2021, where he is currently pursuing the master's degree. He is also engaged in research and development on parallel manipulator, parallel kinematic machine, and their applications.

ZHENLIN JIN was born in Fushun, China, in 1962. He received the Ph.D. degree in mechanical engineering from Yanshan University, China, in 2001. In 2001, he joined the Robotics Research Institute, Beijing University of Aeronautics and Astronautics, as a Postdoctoral Researcher. He is currently a Professor at the School of Mechanical Engineering, Yanshan University. He is also engaged in research and development on novel force sensor with parallel architecture, parallel manipulator, programmable mechanical press, parallel kinematic machine, and their applications.

ZIMING CHEN was born in Hebei, China, in 1984. He received the Ph.D. degree in mechanical engineering from Yanshan University, China, in 2013. From 2017 to 2018, he was a Visiting Scholar at Heriot-Watt University, U.K. He is currently a Professor at the School of Mechanical Engineering, Yanshan University. He is also engaged in research and development on robotics, the theory of parallel robot mechanics and the development of novel parallel equipment.